Quality control of disulfide bond formation in pilus subunits by the chaperone FimC

Crespo, Maria D ; Puorger, Chasper ; Schärer, Martin A ; Eidam, Oliv ; Grütter, Markus G ; Capitani, Guido ; Glockshuber, Rudi

Abstract: Type 1 pili from uropathogenic Escherichia coli are filamentous, noncovalent protein complexes mediating bacterial adhesion to the host tissue. All structural pilus subunits are homologous proteins sharing an invariant disulfide bridge. Here we show that disulfide bond formation in the unfolded subunits, catalyzed by the periplasmic oxidoreductase DsbA, is required for subunit recognition by the assembly chaperone FimC and for FimC-catalyzed subunit folding. FimC thus guarantees quantitative disulfide bond formation in each of the up to 3,000 subunits of the pilus. The X-ray structure of the complex between FimC and the main pilus subunit FimA and the kinetics of FimC-catalyzed FimA folding indicate that FimC accelerates folding of pilus subunits by lowering their topological complexity. The kinetic data, together with the measured in vivo concentrations of DsbA and FimC, predict an in vivo half-life of 2 s for oxidative folding of FimA in the periplasm.

DOI: https://doi.org/10.1038/nchembio.1019

nature chemical biology

ARTICLE

PUBLISHED ONLINE: 1 JULY 2012 | DOI: 10.1038/NCHEMBIO.1019

Quality control of disulfide bond formation in pilus subunits by the chaperone FimC

Maria D Crespo[1], Chasper Puorger[1,5], Martin A Schärer[2,5], Oliv Eidam[3,4], Markus G Grütter[3], Guido Capitani[2,3] & Rudi Glockshuber[1]*

Type 1 pili from uropathogenic *Escherichia coli* are filamentous, noncovalent protein complexes mediating bacterial adhesion to the host tissue. All structural pilus subunits are homologous proteins sharing an invariant disulfide bridge. Here we show that disulfide bond formation in the unfolded subunits, catalyzed by the periplasmic oxidoreductase DsbA, is required for subunit recognition by the assembly chaperone FimC and for FimC-catalyzed subunit folding. FimC thus guarantees quantitative disulfide bond formation in each of the up to 3,000 subunits of the pilus. The X-ray structure of the complex between FimC and the main pilus subunit FimA and the kinetics of FimC-catalyzed FimA folding indicate that FimC accelerates folding of pilus subunits by lowering their topological complexity. The kinetic data, together with the measured *in vivo* concentrations of DsbA and FimC, predict an *in vivo* half-life of 2 s for oxidative folding of FimA in the periplasm.

Type 1 pili from uropathogenic *E. coli* strains are filamentous, highly oligomeric protein complexes anchored to the outer bacterial membrane and are responsible for the attachment of the bacteria to the host tissue[1–3]. Type 1 pili are composed of two different subassemblies: a 1- to 2-μm-long and 7-nm-thick helical, rod-like structure containing up to 3,000 copies of the main structural subunit FimA and a flexible tip fibrillum containing one or several copies of the minor subunits FimG and FimF and a single copy of FimH at the tip of the pilus[2–5] (**Fig. 1a**). Each subunit has an incomplete immunoglobulin-like pilin fold[1] lacking the C-terminal β-strand. In addition, each subunit (except for FimH) has an N-terminal extension ('donor strand'), which is donated to the preceding subunit in the pilus, thereby completing its fold[1,6,7].

Type 1 pili are assembled *in vivo* via the 'chaperone-usher pathway'[8], involving the soluble periplasmic chaperone FimC[9] and the assembly platform ('usher') FimD in the outer membrane[10–12]. The pilus subunits enter the periplasm in an unfolded conformation and are recognized by the chaperone FimC, which catalyzes their folding[13]. FimC also provides a β-strand that complements the fold of the bound subunits and is inserted in a parallel orientation relative to the last (F) strand of the subunit (**Fig. 1b**). The chaperone–subunit complexes then diffuse to the outer membrane usher FimD, where the N-terminal extension of the incoming subunits replaces the donor strand of the chaperone on the previously incorporated subunit at the growing pilus end in a reaction termed donor strand exchange[7,11,14–16]. In contrast to the 'parallel' orientation of the donor strand in FimC–subunit complexes, the donor strand complementing the fold of neighboring subunits in the pilus has an antiparallel orientation relative to the F strand of the acceptor subunit. During pilus assembly *in vivo*, hundreds of donor strand exchange reactions occur on the timescale of several minutes[17,18]. These reactions generate a chain of subunits, which, once translocated through the usher, forms the mature pilus on the surface of the bacterium.

The pilin domains of all pilus subunits contain two cysteine residues that form an invariant structural disulfide bond connecting β-strands A and B (**Fig. 1b**). Several studies have demonstrated the importance of disulfide bond formation in pilus biogenesis[19]. The periplasmic disulfide oxidoreductase DsbA is the principal oxidant of periplasmic proteins with structural disulfide bonds[20,21]. DsbA is essential for the *in vivo* assembly of pili and other disulfide-bonded virulence factors, as deletion of the *dsbA* gene from *E. coli* abolishes pilus biogenesis[22–24].

Here we focus on the initial steps in type 1 pilus assembly, namely binding of the unfolded pilus subunit to the chaperone FimC, followed by chaperone-catalyzed folding. We used the major structural subunit FimA to investigate the role of the disulfide bond in chaperone–subunit (FimC–FimA) complex formation and subunit folding. The disulfide bond in FimA connects residues Cys21 and Cys61, which are situated in the first two β-strands, the A′ strand and the B strand (**Fig. 1b**). Our results show that unfolded, reduced FimA ($FimA^{U}_{red}$) is unable to bind the chaperone and that only unfolded, disulfide-intact FimA ($FimA^{U}_{ox}$) is recognized by FimC. As only FimC-bound subunits are assembly competent[25], this mechanism ensures that each subunit in the assembled pilus has its structural disulfide bond. We determined the crystal structure of FimA bound to FimC and propose a plausible model for FimC-catalyzed subunit folding, in which FimC lowers the topological complexity of the subunits during folding.

RESULTS

FimC only interacts with disulfide-intact unfolded FimA

FimC is a monomeric two-domain protein (22.7 kDa) that interacts with pilus subunits mainly via its N-terminal domain[1,25–27] (the structure of the FimC–FimA complex is described in detail below). The only two tryptophan residues (Trp36 and Trp84) of FimC are located in its N-terminal domain, close to the subunit-binding site. As FimA lacks tryptophan residues, we first tested whether binding of FimA can be detected via a tryptophan fluorescence change in FimC. **Figure 2a** shows that addition of a two-fold excess of $FimA^{U}_{ox}$ to FimC under native conditions resulted in a ~25%

[1]Department of Biology, Institute of Molecular Biology and Biophysics, Swiss Federal Institute of Technology Zurich, Zurich, Switzerland. [2]Laboratory of Biomolecular Research, Paul Scherrer Institute, Villigen, Switzerland. [3]Department of Biochemistry, University of Zurich, Zurich, Switzerland. [4]Present address: Department of Pharmaceutical Chemistry, University of California–San Francisco, San Francisco, California, USA. [5]These authors contributed equally to this work. *e-mail: rudi@mol.biol.ethz.ch

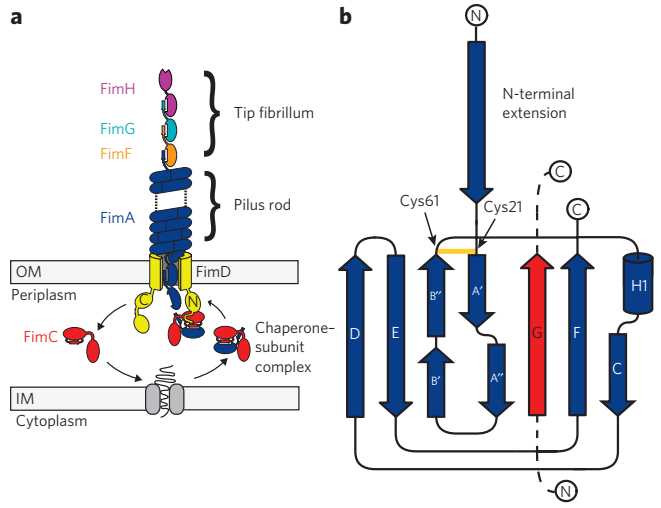

Figure 1 | Schematic of type 1 pilus assembly by the chaperone-usher pathway. (**a**) The periplasmic chaperone FimC forms complexes with the newly translocated pilus subunits (FimA, FimG, FimF and FimH) in the periplasm that diffuse to the assembly platform (usher) FimD. The usher then catalyzes pilus subunit assembly and mediates translocation of folded subunits through the outer membrane[2,10]. Subunits are only assembly competent when bound to FimC[2,10]. OM, outer membrane; IM, inner membrane. (**b**) Topology diagram of the main structural pilus subunit FimA[49]. The location of the single, conserved disulfide bond that connects the N terminus of the first A strand with the C terminus of the second B strand is depicted in yellow with the corresponding residue numbers. The polypeptide segment of FimC that complements the FimA fold in FimC–subunit complexes (donor strand, G strand) is indicated in red.

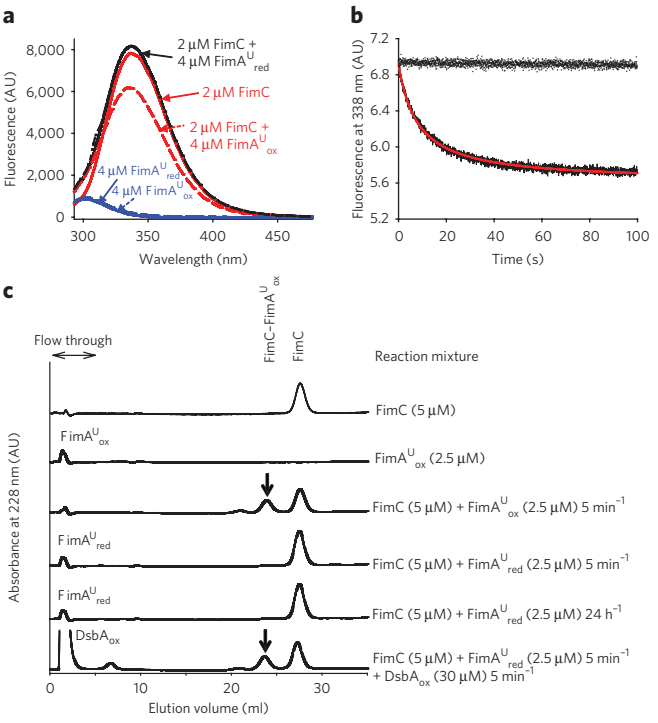

Figure 2 | Complex formation between FimA$^U_{ox}$ and FimC at pH 7.0 and 25 °C. (**a**) Tryptophan fluorescence spectra of 2 μM FimC, 4 μM FimA$^U_{red}$, 4 μM FimA$^U_{ox}$, a mixture of 2 μM FimC and 4 μM FimA$^U_{ox}$ and a mixture of 2 μM FimC and 4 μM FimA$^U_{red}$ (excitation at 280 nm). Dashed black line indicates the sum of the spectra of 2 μM FimC and 4 μM FimA$^U_{red}$. (**b**) Stopped-flow fluorescence kinetics of the refolding of 3 μM FimA$^U_{ox}$ (solid black trace) and 3 μM FimA$^U_{red}$ (dotted black trace) in the presence of 1 equiv. FimC (3 μM FimC). The solid red line represents a fit according to a second-order reaction (equation (1)). (**c**) Analytical ion exchange chromatography of complex formation. FimA$^U_{red}$ or FimA$^U_{ox}$ (2.5 μM) was mixed with a two-fold excess of FimC (5 μM). After incubation for >5 min, the reaction components, FimC, the FimC–FimA complex (arrow) and free FimA were separated by cation exchange chromatography at 4 °C. The identity of the different peaks was verified by SDS-PAGE (**Supplementary Fig. 2**). Addition of DsbA$_{ox}$ to the mixture of FimC and FimA$^U_{red}$ rescued formation of the FimC–FimA complex. Runs with isolated FimA$^U_{ox}$ and isolated FimC are also shown.

decrease in tryptophan fluorescence. Stopped-flow fluorescence kinetics performed with equimolar concentrations of FimC and FimA$^U_{ox}$ proved to be consistent with a bimolecular reaction and yielded a rate constant of 2.91×10^4 M^{-1} s^{-1} for complex formation (**Fig. 2b** and **Supplementary Results**, **Supplementary Table 1**). In contrast, no fluorescence change was observed when FimC was mixed with FimA$^U_{red}$ under the same conditions. As previous experiments had shown that FimC-catalyzed folding of FimA$^U_{ox}$ is completed within less than 1 min under similar experimental conditions[28], we concluded that the decrease in FimC fluorescence upon addition of FimA$^U_{ox}$ results from binding of the unfolded, disulfide-intact subunit and/or subunit folding on the surface of FimC and that FimC is unable to recognize unfolded subunits lacking the disulfide bond. The lack of secondary structure in both FimA$^U_{ox}$ and FimA$^U_{red}$ after the onset of refolding, verified with far-UV CD spectroscopy (**Supplementary Fig. 1**), confirmed that no major structure formation in FimA$^U_{ox}$ is required for recognition by FimC. The reported half-life of 1.6 h (k_f = 0.425 h^{-1}) of spontaneous FimA$^U_{ox}$ folding[28] was confirmed, and spontaneous folding of FimA$^U_{red}$ proceeded even six times slower with a half-life of 9.9 h (k_f = 0.070 h^{-1}) (**Supplementary Fig. 1**).

Oxidation of FimA$^U_{red}$ by DsbA rescues binding to FimC

We next investigated the ability of FimC to selectively bind FimA$^U_{ox}$ using analytical cation-exchange chromatography. This allowed direct detection of the native FimC–FimA complex and the rescuing of unfolded FimA$^U_{red}$ for binding to FimC by oxidation with DsbA. **Figure 2c** shows that FimA$^U_{ox}$ formed a complex with FimC within the dead time of the experiment (about 1 min) after rapid dilution of FimA$^U_{ox}$ into native buffer containing a two-fold excess of FimC. Formation of the FimC–FimA complex was detected via an additional peak and a decrease in the FimC peak intensity (**Fig. 2c** and **Supplementary Fig. 2**). When the same experiment was performed with FimA$^U_{red}$ instead of FimA$^U_{ox}$, no FimC–FimA complex was formed even after incubation for 24 h, and FimA was detected in the flow-through (**Fig. 2c**). However, when an excess of oxidized DsbA (DsbA$_{ox}$) relative to FimA$^U_{red}$ was added to the mixture of FimA$^U_{red}$ and FimC before application to the column, the FimC–FimA complex was fully recovered (**Fig. 2c**). FimA$^U_{red}$ is thus unable to bind FimC, even after prolonged incubation, but is readily converted to its native, FimC-bound and assembly-competent state through oxidation with DsbA. In analogous experiments, we tested whether the ability of the subunit FimG and the pilin domain of FimH (FimH$_p$, residues 160–279) to bind pilus subunits and catalyze their folding was also dependent on disulfide bond formation (**Supplementary Fig. 3a**,**b**). Again, neither unfolded FimG nor unfolded FimH$_p$ bound FimC in the reduced form, but the disulfide-intact subunits quantitatively formed the native FimC–subunit complexes, confirming the requirement of disulfide bond formation for chaperone-catalyzed subunit folding.

Kinetics of DsbA- and FimC-catalyzed FimA folding

The rate constants of oxidation of FimA$^U_{red}$ by DsbA and binding of FimA$^U_{ox}$ to FimC at pH 7.0 were first measured separately under

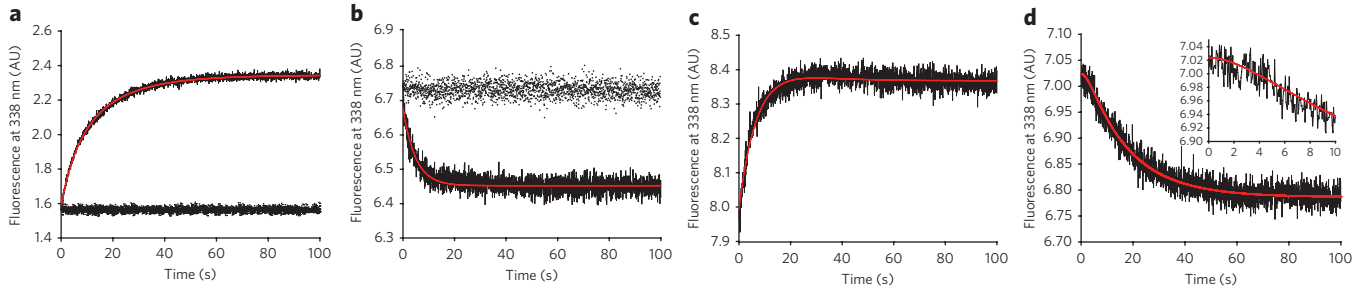

Figure 3 | Stopped-flow fluorescence kinetics of $FimA^{U}_{red}$ oxidation by $DsbA_{ox}$ and subsequent $FimA^{U}_{ox}$ folding and complex formation with FimC (pH 7.0, 25 °C). (**a**) Fluorescence change during oxidation of $FimA^{U}_{red}$ (1 μM) with $DsbA_{ox}$ (5 μM) (solid black trace). No reaction occurs when $FimA^{U}_{ox}$ (1 μM) is mixed with $DsbA_{ox}$ (5 μM) (dotted black trace). The red solid line corresponds to a fit according to a pseudo-first-order reaction. (**b**) Fluorescence decrease upon binding of $FimA^{U}_{ox}$ (1 μM) to FimC (5 μM) (solid black trace). The red, solid line corresponds to a fit according to a pseudo-first-order reaction. As a negative control, the trace for mixing of $FimA^{U}_{red}$ (1 μM) with FimC (5 μM) is also shown (dotted black trace). (**c**) Stopped-flow fluorescence trace of $FimA^{U}_{red}$ refolding (1 μM) in presence of $DsbA_{ox}$ (5 μM) and FimC (5 μM). The reaction is characterized by a fluorescence increase due to formation of reduced DsbA, followed by a fluorescence decrease in FimC due to complex formation with $FimA^{U}_{ox}$ and FimA folding. The solid red line corresponds to a fit according to two consecutive irreversible steps (equation (3)). (**d**) Same reaction as in **c**, but with oxidized $DsbA^{W76F\ W126F}$ instead of $DsbA_{ox}$. Here, the disulfide bond formation step is spectroscopically silent, and subsequent formation of the native FimC–FimA complex becomes evident by a lag phase (inset, reaction between 0 s and 10 s).

pseudo–first-order conditions with fluorescence spectroscopy after stopped-flow mixing. The oxidation of $FimA^{U}_{red}$ (1 μM) with $DsbA_{ox}$ (added in five-fold excess) was traced via the tryptophan fluorescence increase of DsbA upon reduction[29] and yielded a rate constant of $1.56 \times 10^4\ M^{-1}\ s^{-1}$ (**Fig. 3a** and **Supplementary Table 1**). This rate constant is smaller than typical rate constants of polypeptide oxidation by DsbA at pH 7.0, which are in the range of 10^5–$10^7\ M^{-1}\ s^{-1}$ (ref. 30), but is still sufficiently fast to ensure complete oxidation of $FimA^{U}_{red}$ within 100 s under the above conditions (**Fig. 3a**). $FimA^{U}_{ox}$ refolding in the presence of FimC (five-fold excess of FimC over $FimA^{U}_{ox}$) yielded the same rate constant as that measured with equimolar initial concentrations ($k = 2.91 \times 10^4\ M^{-1}\ s^{-1}$; **Fig. 2b**) (**Fig. 3b** and **Supplementary Table 1**).

The kinetics of the combined oxidation and folding reaction were recorded with stopped-flow fluorescence at initial concentrations of 5 μM FimC, 5 μM $DsbA_{ox}$ and 1 μM $FimA^{U}_{red}$, and the fluorescence change was analyzed according to two consecutive, irreversible steps (equation (3); **Fig. 3c**). The obtained rate constants were identical within experimental error to those obtained for the independent reactions (**Supplementary Table 1**) and confirmed that FimC-catalyzed folding ($k = 2.83 \times 10^4\ M^{-1}\ s^{-1}$) proceeded slightly faster than the oxidation reaction with DsbA ($k = 1.23 \times 10^4\ M^{-1}\ s^{-1}$).

The two reactions, oxidation and complex formation, have opposite signal changes, with two spectroscopic probes, DsbA and FimC, contributing to the change in tryptophan fluorescence. To verify this sequential mechanism, we used a spectroscopically silent variant of DsbA, $DsbA^{W76F\ W126F}_{ox}$ with wild-type–like catalytic properties[31], which allowed selective observation of FimC-mediated FimA folding. The data confirmed the sequential mechanism in which oxidation must precede folding, as we observed the predicted lag phase of about 2 s for the decrease in FimC fluorescence upon binding and folding of $FimA^{U}_{ox}$ (**Fig. 3d**).

Binding of $FimA^{U}_{ox}$ rate-limits FimC-catalyzed folding

The FimC fluorescence decrease observed after mixing with $FimA^{U}_{ox}$ may be due to $FimA^{U}_{ox}$ folding on the surface of FimC or caused by binding of $FimA^{U}_{ox}$. To resolve this mechanistic question, we applied two strategies. First, we performed interrupted refolding experiments, which allow direct monitoring of native FimA molecules[32], as the native (denoted by superscript N) FimC–$FimA^{N}_{ox}$ complexes are more resistant against dissociation by denaturants than FimC–$FimA^{U}_{ox}$ complexes. Second, we refolded $FimA^{U}_{ox}$ in the presence of FimC under pseudo–first-order conditions (constant four-fold excess of FimC), but we varied the total protein concentration over a factor of 16. As the rate of binding of $FimA^{U}_{ox}$ to FimC is concentration dependent and folding of $FimA^{U}_{ox}$ on the FimC surface is concentration independent, we expected the rate of FimC-catalyzed folding at higher total protein concentrations to be faster if binding of $FimA^{U}_{ox}$ was rate-limiting for catalysis.

Figure 4a shows the fluorescence traces of an interrupted refolding experiment in which $FimA^{U}_{ox}$ (2.5 μM) was first mixed with an excess of FimC (10 μM). The refolding reaction was then interrupted after different times by addition of guanidinium chloride (GdmCl) to a final concentration of 0.7 M GdmCl to induce complex dissociation and unfolding of $FimA^{N}_{ox}$. In addition to the

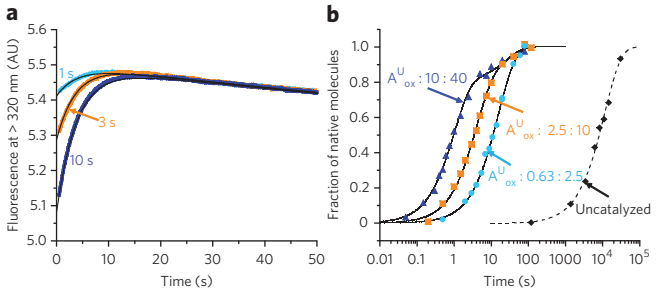

Figure 4 | Kinetics of FimC-catalyzed folding of $FimA^{U}_{ox}$ at pH 7.0, 25 °C, showing that binding of $FimA^{U}_{ox}$ is the rate-limiting step in the formation of the native FimC-FimA complex. (**a**) Examples of fluorescence traces from interrupted refolding experiments. $FimA^{U}_{ox}$ (2.5 μM) was mixed with a four-fold excess of FimC. The reaction was stopped after different times by adding GdmCl (final concentration 0.7 M), which caused dissociation and unfolding. Unfolding traces after refolding for 1 s, 3 s and 10 s are shown. (**b**) Kinetics of FimC-catalyzed folding of $FimA^{U}_{ox}$, detected by interrupted refolding experiments. FimC-catalyzed folding was performed at a constant $FimA^{U}_{ox}$-to-FimC ratio of 1:4 but at different total protein concentrations: 0.63 μM $FimA^{U}_{ox}$/2.5 μM FimC, 2.5 μM $FimA^{U}_{ox}$/10 μM FimC and 10 μM $FimA^{U}_{ox}$/40 μM FimC. The solid black lines (labeled with the corresponding FimC and $FimA^{U}_{ox}$ concentrations in μM) represent a global fit of the data with a biexponential equation (equation (8); **Supplementary Methods**) accounting for 20% of slow-folding $FimA^{U}_{ox}$ molecules due to accumulation of non-native *cis*-prolyl peptide bonds in the presence of denaturant. The spontaneous folding of $FimA^{U}_{ox}$ in the absence of FimC (black diamonds) shows monoexponential kinetics (dashed line) with a half-life of 1.6 h and is not limited by prolyl peptide bond isomerization.

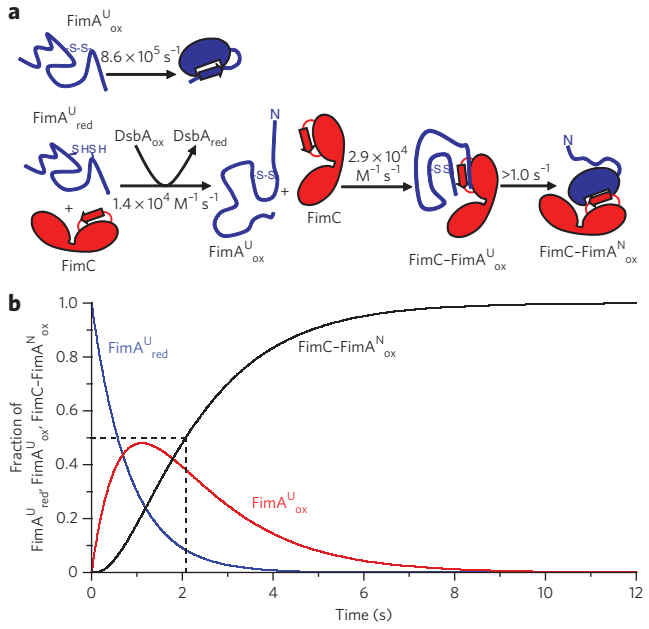

Figure 5 | Mechanism and *in vivo* kinetics of DsbA- and FimC-catalyzed folding of FimA. (**a**) Comparison between uncatalyzed folding of FimA$^{U}_{ox}$ with the sequential mechanism of DsbA- and FimC-catalyzed oxidative folding of FimA$^{U}_{red}$. (**b**) Simulation of the kinetics of DsbA- and FimC-catalyzed oxidative folding of FimA *in vivo*. The fraction of FimA$^{U}_{red}$, FimA$^{U}_{ox}$ and the native FimC–FimA$^{N}_{ox}$ complex at periplasmic DsbA and FimC concentrations of 86 μM and 23 μM, respectively, is plotted against folding time, assuming that both DsbA$_{ox}$ and FimC are present at excess over FimA$^{U}_{red}$ molecules newly entering the periplasm via the Sec translocon. The dashed line indicates the deduced *in vivo* half-life of ~2.1 s for formation of the FimC–FimA$^{N}_{ox}$ complex.

expected increase in fluorescence due to dissociation of FimA from FimC, we also observed a slower second phase with a decrease in tryptophan fluorescence, which could be attributed to the slow unfolding of about 10% of the FimC molecules at 0.7 M GdmCl (**Supplementary Fig. 4**). In summary, the increase in amplitudes of the faster phase (measuring FimC fluorescence increase) directly reported on the fraction of native FimA molecules bound to FimC after different reaction times.

Figure 4b shows the deduced kinetics of formation of native FimC–FimA$^{N}_{ox}$ complexes at three different concentrations of FimA (0.63 μM, 2.5 μM and 10 μM) and with a constant, four-fold excess of FimC over FimA. The globally fitted data (**Supplementary Table 2**) were indeed fully consistent with a bimolecular reaction mechanism, in which the pseudo–first-order rate of FimC-catalyzed folding of FimA$^{U}_{ox}$ increased linearly with total protein concentration. Consequently, binding of FimA$^{U}_{ox}$ by FimC, and not folding of FimC-bound FimA, is the rate-limiting step in FimC-catalyzed subunit folding. The deduced second-order rate constant of 2.59 × 10^{4} M^{-1} s^{-1} for formation of native molecules is in agreement with the rate constants obtained from recording the fluorescence decrease in FimC upon addition of FimA$^{U}_{ox}$.

Figure 4b also shows that a biexponential function in global data fitting (equation (8)) had to be used to account for 20 ± 2.5% of slow-folding FimA species, which became evident at the two highest protein concentrations used (**Fig. 4b** and **Supplementary Table 2**). We interpret the slow-folding species as an *in vitro* folding artifact caused by the *cis*-to-*trans* isomerization of non-native *cis*-prolyl peptide bonds that accumulate in FimA$^{U}_{ox}$ upon long-term incubation in denaturant; as the only two prolyl peptide bonds (isoleucine-proline and threonine-proline) in FimA are in the *trans* conformation in the native state[28], 20% of FimA$^{U}_{ox}$ molecules with at least one non-native *cis*-prolyl peptide bond is indeed predicted for unfolded FimA on the basis of studies on unstructured model peptides[33]. In addition, the slower phase in **Figure 4b** shows a concentration-independent half-life of 18 s (**Supplementary Table 2**), which is in the typical range for a prolyl *cis*-to-*trans* isomerization at 25 °C[34].

Together, the results show that binding of unfolded FimA$_{ox}$ to FimC is the rate-limiting step in the formation of folded FimA$_{ox}$ under the given experimental conditions. Hence, FimA$_{ox}$ folding on the surface of FimC must be faster than the fastest observed rate ($k_{\text{catalyzed folding}}$ > 1 s^{-1}). As noncatalyzed folding of FimA$^{U}_{ox}$ is a very slow process with a folding rate constant of 8.63 × 10^{-5} s^{-1} (**Fig. 4b**)[28], FimC accelerates folding of FimA$^{U}_{ox}$ by at least four orders of magnitude.

Catalyzed FimA folding *in vivo*

Figure 5a summarizes the consecutive mechanism of DsbA- and FimC-catalyzed FimA folding *in vitro*. We next used the measured second-order rate constants of FimA oxidation and binding to FimC to predict the *in vivo* half-life of oxidative FimA folding and the extent to which FimA$^{U}_{ox}$ would accumulate as a folding intermediate in the periplasm. For this purpose, we determined the *in vivo* concentrations of DsbA and FimC in the *E. coli* K12 wild-type strain W3110 by quantitative western blotting (**Supplementary Fig. 5**). Assuming a periplasmic volume of 6.5 × 10^{-17} l, corresponding to ~9.3% of the total cell's aqueous volume (*E. coli* statistics: http://ccdb.wishartlab.com/CCDB/cgi-bin/STAT_NEW.cgi), we obtained counts of ~3.4 × 10^{3} DsbA molecules and ~920 FimC molecules per *E. coli* cell at mid–log phase, which translate into periplasmic concentrations of ~86 μM and ~23 μM of DsbA$_{ox}$ and FimC, respectively (DsbA has been shown to be fully oxidized *in vivo* under aerobic conditions[35]). Assuming an excess of periplasmic DsbA$_{ox}$ and FimC over FimA$^{U}_{red}$ molecules newly entering the periplasm (that is, pseudo–first-order conditions), we were able to predict an *in vivo* half-life of 2.1 s for formation of native FimC–FimA complexes (**Fig. 5b**). Oxidative folding of FimA *in vivo* is thus clearly faster than in our *in vitro* experiment (**Fig. 3c**), where we observed a half-life of about 20 s with identical initial concentrations of 5 μM for DsbA$_{ox}$ and FimC. Although the periplasmic concentrations of FimC and DsbA might be subject to variations in the volume of the periplasm, it is nevertheless safe to state that FimA$^{U}_{red}$ becomes rapidly oxidized by DsbA *in vivo* on the timescale of seconds and that FimA$^{U}_{ox}$ does not accumulate to more than 50%, as it is rapidly bound by FimC (**Fig. 5b**). This fast binding to FimC *in vivo* may be responsible for the reported protection against degradation of pilus subunits by pilus chaperones[36].

FimC–FimA$_t$ structure

Recently, we reported the NMR structure of a designed, self-complemented FimA variant (FimAa)[28], in which FimA is artificially extended at its C terminus by a hexaglycine linker followed by the FimA donor strand segment (residues 1–20). FimAa has the same slow, spontaneous folding rate as wild-type FimA (1.6-h folding half-life) and adopts a conformation in which the C-terminal copy of the donor strand is incorporated into the tertiary structure in an antiparallel orientation relative to the FimA F strand, which corresponds to the expected donor strand insertion pattern in the quaternary structure of the pilus rod[28]. To unravel the structural basis of the at least 10^{4}-fold acceleration of FimA folding upon binding to FimC, we solved the X-ray structure of the FimC–FimA complex at 2.5-Å resolution and compared it with the structure of FimA$_a$. To prevent formation of FimA homopolymers[28], we used an N-terminally truncated FimA variant (FimA$_t$) lacking residues 1–17 of FimA[14,28] and bearing an uncleaved methionine at the N terminus. **Figure 6a** provides an overall representation of the FimC–FimA$_t$ structure and

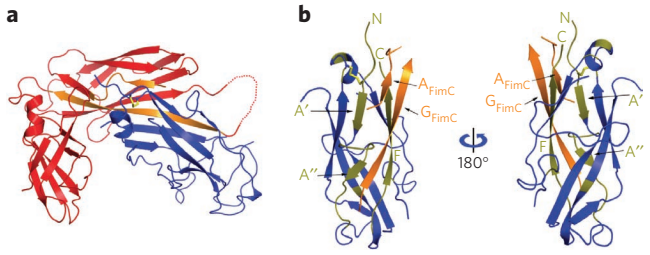

Figure 6 | 2.5-Å X-ray structure of the FimC–$FimA_t$ complex. (**a**) Cartoon representation of the complex, with FimC in red and $FimA_t$ in blue. The donor strand (G strand) and the A strand of FimC interacting with the A′ strand of $FimA_t$ appear in orange. The disulfide bond of $FimA_t$ in the 2.5-Å structure is clearly visible and is shown in stick representation (yellow). (**b**) Close-up view of the $FimA_t$ subunit. $FimA_t$ residues interacting with FimC (as determined with the program CONTACT of the CCP4 suite[50] using a 4-Å cut off) are colored in olive (**Supplementary Fig. 6**).

refers to the first (chains A and B) of the two complexes found in the asymmetric unit. The structure has very good geometry and stereochemistry (**Supplementary Table 3**), with only few residues absent from the model owing to disorder (FimC residues 95–99 and 205 and $FimA_t$ residues 91–94 and 121–126).

The FimC-subunit interaction is similar to that observed in the FimC–FimH complex[1] and the FimC–FimF complex[26] (**Supplementary Figs. 6** and **7**). The chaperone inserts residues 101–110 into FimA in a parallel orientation to the F strand of FimA and thereby complements the FimA pilin fold (**Fig. 6a**,**b**). The interface area between the two molecules is 1,691 $Å^2$, as determined with PISA[37]. The Cα r.m.s. deviation between FimC–$FimA_t$ and FimC–FimH (from the structure of the ternary FimC–FimH–FimD complex, Protein Data Bank (PDB) code 1ZE3 (ref. 25)) is 1.31 Å (0.99 Å after optimization of the rotation matrix and vector, measured over 225 equivalent Cα atoms within 1.9 Å), whereas the Cα r.m.s. deviation with FimC–FimF (from the structure of the ternary FimC–FimF–FimD complex, PDB code 3BWU[26]) is 1.07 Å (0.77 Å after optimization, measured over 235 equivalent Cα atoms). R.m.s. deviation values were calculated with Superimpose[38].

Side chain interactions between the $FimA_t$ and FimC cluster at the N and C terminus of the $FimA_t$ sequence (**Supplementary Fig. 6**) and are of predominantly polar character. At the C terminus, $FimA_t$ residues 147–159 (containing the F strand) interact with FimC via 15 hydrogen bonds, 9 of which are exclusively between main-chain atoms, as determined with HBPLUS[39]. In addition, the carboxyl group of the C-terminal Gln159 forms two salt bridges with Arg8 and Lys112, two invariant residues located in the interdomain cleft of the chaperone. Mutations of the corresponding residues studied in PapD, a close homolog of FimC, revealed that both residues are critical for pilus subunit binding[40]. The N-terminal region of $FimA_t$, including the A′ strand, interacts with residues 1–7 of FimC, whereas the A′ strand forms an antiparallel β-sheet with the G strand of FimC. Sixteen intermolecular hydrogen bonds (eight of which are main-chain only) and one salt bridge (between Asp24 of FimA and the N-terminal amino group of FimC) are formed by the FimA segment encompassing residues 17–37. The FimA disulfide bond is solvent inaccessible, in agreement with the requirement of DsbA-catalyzed disulfide bond formation before FimA folding.

Superposition of $FimA_a$ (PDB code 2JTY[28], conformer 18, as selected by OLDERADO[41]) over $FimA_t$ in the FimC–FimA complex (chain B, **Supplementary Fig. 8**) shows that the structures are similar, with 95 equivalent Cα atoms (within 1.9 Å) aligning with a mean r.m.s. deviation of 1.18 Å. A total of 113 residues , corresponding to more than 80% of the $FimA_t$ sequence, align within 2.5 Å. The r.m.s. deviation over the whole $FimA_t$ structure (residues 18–159) is 2.68 Å, as calculated with LSQKAB[42]. The most prominent differences between the two structures are the sequence and orientation of the donor strand complementing the subunit fold: the G strand of $FimA_a$ (corresponding to the natural N-terminal extension of FimA) runs antiparallel to the F strand, whereas the donor strand of FimC (**Fig. 6a**,**b**) runs parallel to it. Further structural differences are found at the N terminus and between residues 24 and 29, where a short helix is formed in the $FimA_a$ structure. Residues 63–67 form a helix in $FimA_t$ but not in $FimA_a$. Substantial deviations are also observed between residues 119 and 128. However, as reflected by the low r.m.s. deviation, most β-strands and loops superimpose well (**Supplementary Fig. 8**).

DISCUSSION

It is well established that DsbA is the main oxidant of thiol pairs in the periplasm[20]. Several studies have shown a negative effect of a *dsbA* deletion background on bacterial pathogenicity[19,43,44]. The deletion of the *dsbA* gene on the *E. coli* genome leads to the complete absence of type 1 pili[22]. Only when the entire type 1 pilus gene cluster was overexpressed via a plasmid in a *dsbA* deletion strain could type 1 pilus biogenesis still be observed, but at reduced levels compared to wild-type cells[23,24]. The latter finding does not contradict the dependence on DsbA of type 1 pilus biogenesis in wild-type *E. coli* strains and may be explained by partial oxidation of overexpressed pilus subunits by air oxygen, which is possibly catalyzed by traces of transition metals such as copper[45]. The periplasmic disulfide isomerase DsbC might also act as an oxidant under certain growth conditions[19,20,46]. In the case of the homologous P pilus system, pilus assembly was also abolished in a strain lacking DsbA. The effect of the *dsbA* deletion on P pilus assembly had been interpreted such that the single structural disulfide bond between Cys228 and Cys233 in the P pilus chaperone PapD would no longer form in the absence of DsbA, thereby preventing PapD folding and thus pilus biogenesis[23]. The results obtained in this study reveal that disulfide bond formation has a much more profound function in pilus assembly than previously assumed. First, the type 1 pilus chaperone FimC lacks cysteines, so the lack of disulfide bond formation only affects the folding of the type 1 pilus subunits. Second, and most importantly, we showed that unfolded pilus subunits cannot be recognized by FimC unless the disulfide bond in the subunit is already formed. Thus, pilus subunit folding in the periplasm cannot be catalyzed by FimC when the only physiological oxidant, DsbA, is missing, and the pilus subunit will not become assembly competent. Third, it is essential that all subunits in a supramolecular unit such as the type 1 pilus rod have the same high stability. Only a single, unstable subunit lacking the structural disulfide bond in the pilus rod, which consists of up to 3,000 FimA copies, might lead to the dissociation of the rod in the extracellular space, in particular under shear forces[47]. FimC thus has a previously unknown quality control function for disulfide bond formation in each subunit and ensures that only oxidized subunits are incorporated into the pilus. FimC is also unique in that it is the only folding catalyst described so far that is strictly dependent on disulfide bond formation in the polypeptide substrate.

Our results, together with previous reports[13,23,24,48], suggest a straightforward model for the FimC-catalyzed subunit folding of FimA and other pilus subunits. As the FimA fold has a high topological complexity (contact order)[28], this might be the dominant factor determining the high kinetic barrier of spontaneous FimA folding. We propose that FimC lowers this kinetic barrier via a mechanism consistent with the interactions between FimC and FimA in the FimC–$FimA_t$ structure. As FimC neither catalyzes folding of reduced FimA nor forms complexes with $FimA^U_{red}$, it is evident that the hairpin formed by strands A′, A″ and B, held together at its base by the disulfide bridge, is a recognition unit for FimC. The contact area between FimC and this recognition unit is 745 A^2.

Another key binding motif, first identified in the complex between the PapD chaperone and a C-terminal peptide of the subunit PapG[40], is the C-terminal F strand of the pilin domain. This F strand–chaperone interaction is also conserved in all structures of FimC–subunit complexes[1,25,26]. As the A′, A″ and F strands are the N- and C-terminal FimA segments, respectively, their simultaneous binding to the donor strand (G strand) of FimC leads to 'circularization' of the FimA polypeptide chain (**Supplementary Fig. 9**). The circularization predicts a dramatic reduction of topological complexity for the folding process so that the rest of the pilin chain might rapidly collapse to the native structure.

Kinetic simulations performed with the determined *in vivo* concentrations of DsbA and FimC provide strong hints that DsbA- and FimC-dependent *in vivo* folding of FimA proceeds rapidly, with a deduced *in vivo* half-life of about 2 s. Although the situation *in vivo* is more complex than in our *in vitro* experiments (there is competition between multiple periplasmic polypeptide substrates for oxidation by DsbA), we are convinced that the simulated *in vivo* populations of FimA species and the timescale of FimA folding *in vivo* (**Fig. 5b**) are reasonable estimates. Our approach for determination of *in vivo* folding rates based on the *in vivo* concentrations of essential folding catalysts and their rate constants of interaction with polypeptide substrates measured *in vitro* should be generally applicable to predict *in vivo* folding rates of proteins that require catalysts for efficient folding.

METHODS

Protein expression and purification. A FimC variant with a C-terminal His_6 tag ($FimC_{His}$)[13] was used in the biochemical experiments. $FimC_{His}$, $FimA^U_{ox}$, $DsbA_{ox}$ and $DsbA^{W76F\ W126F}_{ox}$ were expressed and purified as previously described[13,28,29,31]. Protein concentrations were determined via the molar extinction coefficients at 280 nm ($FimC_{His}$: 22,900 M^{-1} cm^{-1}, $FimA^U_{ox}$: 3,105 M^{-1} cm^{-1}, $DsbA_{ox}$: 23,045 M^{-1} cm^{-1}, $DsbA^{W76F\ W126F}_{ox}$: 12,045 M^{-1} cm^{-1}).

For production of $FimA^U_{red}$, native FimA (200 µM) was incubated in 6 M GdmCl and 50 mM sodium phosphate pH 7.0 for 1 h at 37 °C with 100 mM dithiothreitol and applied to a HiTrap desalting column (GE Healthcare) equilibrated with 6 M GdmCl and 10 mM potassium acetate pH 4.5 to remove the dithiothreitol. The obtained stock solution of $FimA^U_{red}$ was buffer exchanged with 50 mM sodium phosphate pH 7.0 before fluorescence measurements.

Refolding experiments. All experiments were performed in 50 mM sodium phosphate pH 7.0 at 25 °C. Equilibrium fluorescence spectra were measured on a QM-7/2003 spectrofluorimeter (PTI). Kinetic experiments were performed on an SX18.MV stopped-flow instrument (Applied Photophysics). Single-wavelength scans were performed at an excitation wavelength of 280 nm. Single-jump kinetics were initiated by 1:1 mixing of FimC or FimC/$DsbA_{ox}$ or FimC/$DsbA^{W76F\ W126F}_{ox}$ with either $FimA^U_{ox}$ or $FimA^U_{red}$ and were monitored by the change in tryptophan fluorescence at 338 nm.

The kinetics of the change in FimC tryptophan fluorescence upon FimA binding and folding was fitted with an equation describing a bimolecular reaction

$$I = I_0 - \Delta I \frac{(A_0 - C_0)\exp(-k_{on}(A_0 - C_0)t)}{A_0 - C_0\exp(-k_{on}(A_0 - C_0)t)} \quad (1)$$

where I_0 is the initial fluorescence intensity, ΔI is the amplitude of FimC fluorescence change upon binding of $FimA^U_{ox}$ to FimC and FimC-catalyzed FimA folding, and A_0 and C_0 are the initial concentrations of $FimA^U_{ox}$ and FimC.

The consecutive kinetic mechanism of $FimA^U_{red}$ oxidation by $DsbA_{ox}$ followed by FimC-catalyzed folding was analyzed according to

$$A \xrightarrow{k_1} B \xrightarrow{k_2} C \quad (2)$$

where A, B and C are the reaction mixtures of $FimA^U_{red}$ plus $FimC_{His}$ plus $DsbA_{ox}$, $FimA^U_{ox}$ plus $FimC_{His}$ plus $DsbA_{red}$ and $FimC_{His}$–$FimA^N_{ox}$ plus $DsbA_{red}$, contributing to the fluorescence signal in the initial, intermediate and final state of the sequential mechanism, respectively, and k_1 and k_2 are the pseudo–first-order rate constants of the corresponding reactions.

Fluorescence traces were fitted with the following equation:

$$F_{obs} = F_A\gamma_A + F_B\gamma_B + F_C\gamma_C \quad (3)$$

where F_{obs} is the observed fluorescence and F_A, F_B and F_C are the fluorescence signals of the reaction mixtures $FimA^U_{red}$ plus $FimC_{His}$ plus $DsbA_{ox}$, $FimA^U_{ox}$ plus $FimC_{His}$ plus $DsbA_{red}$ and $FimC_{His}$–$FimA^N_{ox}$ plus $DsbA_{red}$, respectively. The fractions of A, B and C (γ_A, γ_B and γ_C) were obtained from the following equations:

$$\gamma_A = \exp(-k_1 t) \quad (4)$$

$$\gamma_B = \frac{k_1}{k_2 - k_1}\left[\exp(-k_1 t) - \exp(-k_2 t)\right] \quad (5)$$

$$\gamma_C = 1 + \frac{1}{k_1 - k_2}\left[k_2\exp(-k_1 t) - k_1\exp(-k_2 t)\right] \quad (6)$$

The change in FimC tryptophan fluorescence at 338 nm upon refolding of FimA in the presence of FimC was recorded at an excitation wavelength of 280 nm and analyzed using Berkeley Madonna 8.3 (Macey & Oster).

Interrupted refolding experiments. The formation of $FimA^N_{ox}$–FimC complexes during refolding of $FimA^U_{ox}$ in the presence of FimC at pH 7.0 and 25 °C was detected by interrupted refolding experiments, in which the refolding reaction was stopped after different times by addition of GdmCl to a final concentration of 0.7 M, which caused complex dissociation and unfolding of $FimA^N_{ox}$. The fraction of native complexes after each refolding time was then quantified by the fluorescence amplitude of the unfolding and dissociation phase. A detailed description of the experimental setup and data evaluation is provided in the **Supplementary Methods**.

Analytical, fast ion-exchange chromatography. $FimA^U_{ox}$ or $FimA^U_{red}$ (2.5 µM) was incubated in the presence of a two-fold excess of FimC (5 µM) for >5 min in 10 mM sodium phosphate pH 7.0 and 200 mM NaCl, and the reaction mixture was applied to fast cation exchange chromatography at 4 °C using a 1-ml Resource S column (GE Healthcare) equilibrated with 20 mM MOPS adjusted to pH 6.7 with NaOH. The reaction products were separated with a NaCl gradient and detected at 228 nm. A 12-fold molar excess of $DsbA_{ox}$ over $FimA^U_{red}$ was added to the mixture of FimC and $FimA^U_{red}$ before the fast cation exchange chromatography.

Determination of the periplasmic concentrations of DsbA and FimC. Protocols for quantitative western blotting and calibration curves are provided in the **Supplementary Methods**.

Crystallization and structure determination. Protocols are provided in the **Supplementary Methods**.

Accession codes. PDB: The coordinates and structure factors of the FimC–$FimA_t$ complex have been deposited under accession code 4DWH.

Received 16 April 2012; accepted 5 June 2012; published online 1 July 2012

References

1. Choudhury, D. *et al.* X-ray structure of the FimC-FimH chaperone-adhesin complex from uropathogenic *Escherichia coli*. *Science* **285**, 1061–1066 (1999).
2. Hahn, E. *et al.* Exploring the 3D molecular architecture of *Escherichia coli* type 1 pili. *J. Mol. Biol.* **323**, 845–857 (2002).
3. Jones, C.H. *et al.* FimH adhesin of type 1 pili is assembled into a fibrillar tip structure in the Enterobacteriaceae. *Proc. Natl. Acad. Sci. USA* **92**, 2081–2085 (1995).
4. Le Trong, I. *et al.* Donor strand exchange and conformational changes during *E. coli* fimbrial formation. *J. Struct. Biol.* **172**, 380–388 (2010).
5. Le Trong, I. *et al.* Structural basis for mechanical force regulation of the adhesin FimH via finger trap-like β-sheet twisting. *Cell* **141**, 645–655 (2010).
6. Sauer, F.G. *et al.* Structural basis of chaperone function and pilus biogenesis. *Science* **285**, 1058–1061 (1999).
7. Sauer, F.G., Pinkner, J.S., Waksman, G. & Hultgren, S.J. Chaperone priming of pilus subunits facilitates a topological transition that drives fiber formation. *Cell* **111**, 543–551 (2002).
8. Hung, D.L., Knight, S.D., Woods, R.M., Pinkner, J.S. & Hultgren, S.J. Molecular basis of two subfamilies of immunoglobulin-like chaperones. *EMBO J.* **15**, 3792–3805 (1996).
9. Jones, C.H. *et al.* FimC is a periplasmic PapD-like chaperone that directs assembly of type 1 pili in bacteria. *Proc. Natl. Acad. Sci. USA* **90**, 8397–8401 (1993).
10. Nishiyama, M., Ishikawa, T., Rechsteiner, H. & Glockshuber, R. Reconstitution of pilus assembly reveals a bacterial outer membrane catalyst. *Science* **320**, 376–379 (2008).
11. Phan, G. *et al.* Crystal structure of the FimD usher bound to its cognate FimC-FimH substrate. *Nature* **474**, 49–53 (2011).

12. Saulino, E.T., Thanassi, D.G., Pinkner, J.S. & Hultgren, S.J. Ramifications of kinetic partitioning on usher-mediated pilus biogenesis. *EMBO J.* **17**, 2177–2185 (1998).
13. Vetsch, M. *et al.* Pilus chaperones represent a new type of protein-folding catalyst. *Nature* **431**, 329–333 (2004).
14. Vetsch, M. *et al.* Mechanism of fibre assembly through the chaperone-usher pathway. *EMBO Rep.* **7**, 734–738 (2006).
15. Remaut, H. *et al.* Donor-strand exchange in chaperone-assisted pilus assembly proceeds through a concerted beta strand displacement mechanism. *Mol. Cell* **22**, 831–842 (2006).
16. Zavialov, A.V. *et al.* Structure and biogenesis of the capsular F1 antigen from *Yersinia pestis*: preserved folding energy drives fiber formation. *Cell* **113**, 587–596 (2003).
17. Dodd, D.C. & Eisenstein, B.I. Kinetic analysis of the synthesis and assembly of type 1 fimbriae of *Escherichia coli*. *J. Bacteriol.* **160**, 227–232 (1984).
18. Jacob-Dubuisson, F., Striker, R. & Hultgren, S.J. Chaperone-assisted self-assembly of pili independent of cellular energy. *J. Biol. Chem.* **269**, 12447–12455 (1994).
19. Heras, B. *et al.* DSB proteins and bacterial pathogenicity. *Nat. Rev. Microbiol.* **7**, 215–225 (2009).
20. Hiniker, A. & Bardwell, J.C. *In vivo* substrate specificity of periplasmic disulfide oxidoreductases. *J. Biol. Chem.* **279**, 12967–12973 (2004).
21. Bardwell, J.C., McGovern, K. & Beckwith, J. Identification of a protein required for disulfide bond formation *in vivo*. *Cell* **67**, 581–589 (1991).
22. Bringer, M.A., Rolhion, N., Glasser, A.L. & Darfeuille-Michaud, A. The oxidoreductase DsbA plays a key role in the ability of the Crohn's disease-associated adherent-invasive *Escherichia coli* strain LF82 to resist macrophage killing. *J. Bacteriol.* **189**, 4860–4871 (2007).
23. Jacob-Dubuisson, F. *et al.* PapD chaperone function in pilus biogenesis depends on oxidant and chaperone-like activities of DsbA. *Proc. Natl. Acad. Sci. USA* **91**, 11552–11556 (1994).
24. Totsika, M., Heras, B., Wurpel, D.J. & Schembri, M.A. Characterization of two homologous disulfide bond systems involved in virulence factor biogenesis in uropathogenic *Escherichia coli* CFT073. *J. Bacteriol.* **191**, 3901–3908 (2009).
25. Nishiyama, M. *et al.* Structural basis of chaperone-subunit complex recognition by the type 1 pilus assembly platform FimD. *EMBO J.* **24**, 2075–2086 (2005).
26. Eidam, O., Dworkowski, F.S., Glockshuber, R., Grutter, M.G. & Capitani, G. Crystal structure of the ternary FimC-$FimF_t$-$FimD_N$ complex indicates conserved pilus chaperone-subunit complex recognition by the usher FimD. *FEBS Lett.* **582**, 651–655 (2008).
27. Pellecchia, M., Sebbel, P., Hermanns, U., Wuthrich, K. & Glockshuber, R. Pilus chaperone FimC-adhesin FimH interactions mapped by TROSY-NMR. *Nat. Struct. Biol.* **6**, 336–339 (1999).
28. Puorger, C., Vetsch, M., Wider, G. & Glockshuber, R. Structure, folding and stability of FimA, the main structural subunit of type 1 pili from uropathogenic *Escherichia coli* strains. *J. Mol. Biol.* **412**, 520–535 (2011).
29. Wunderlich, M. & Glockshuber, R. Redox properties of protein disulfide isomerase (DsbA) from *Escherichia coli*. *Protein Sci.* **2**, 717–726 (1993).
30. Wunderlich, M., Otto, A., Seckler, R. & Glockshuber, R. Bacterial protein disulfide isomerase: efficient catalysis of oxidative protein folding at acidic pH. *Biochemistry* **32**, 12251–12256 (1993).
31. Hennecke, J., Sillen, A., Huber-Wunderlich, M., Engelborghs, Y. & Glockshuber, R. Quenching of tryptophan fluorescence by the active-site disulfide bridge in the DsbA protein from *Escherichia coli*. *Biochemistry* **36**, 6391–6400 (1997).
32. Schmid, F.X. Mechanism of folding of ribonuclease A. Slow refolding is a sequential reaction via structural intermediates. *Biochemistry* **22**, 4690–4696 (1983).
33. Reimer, U. *et al.* Side-chain effects on peptidyl-prolyl cis/trans isomerisation. *J. Mol. Biol.* **279**, 449–460 (1998).
34. Balbach, J. & Schmid, F.X. Prolyl isomerization and its catalysis in protein folding in *Mechanisms of Protein Folding: Frontiers in Molecular Biology* 2nd edn. (ed. Pain, R.H.) 212–249 (Oxford University Press, 2000).
35. Kobayashi, T. & Ito, K. Respiratory chain strongly oxidizes the CXXC motif of DsbB in the *Escherichia coli* disulfide bond formation pathway. *EMBO J.* **18**, 1192–1198 (1999).
36. Barnhart, M.M. *et al.* PapD-like chaperones provide the missing information for folding of pilin proteins. *Proc. Natl. Acad. Sci. USA* **97**, 7709–7714 (2000).
37. Krissinel, E. & Henrick, K. Inference of macromolecular assemblies from crystalline state. *J. Mol. Biol.* **372**, 774–797 (2007).
38. Diederichs, K. Structural superposition of proteins with unknown alignment and detection of topological similarity using a six-dimensional search algorithm. *Proteins* **23**, 187–195 (1995).
39. McDonald, I.K. & Thornton, J.M. Satisfying hydrogen bonding potential in proteins. *J. Mol. Biol.* **238**, 777–793 (1994).
40. Kuehn, M.J. *et al.* Structural basis of pilus subunit recognition by the PapD chaperone. *Science* **262**, 1234–1241 (1993).
41. Kelley, L.A. & Sutcliffe, M.J. OLDERADO: on-line database of ensemble representatives and domains. On line database of ensemble representatives and domains. *Protein Sci.* **6**, 2628–2630 (1997).
42. Kabsch, W. A solution for the best rotation to relate two sets of vectors. *Acta Crystallogr. A* **32**, 922–923 (1976).
43. Łasica, A.M. & Jagusztyn-Krynicka, E.K. The role of Dsb proteins of Gram-negative bacteria in the process of pathogenesis. *FEMS Microbiol. Rev.* **31**, 626–636 (2007).
44. Yu, J. & Kroll, J.S. DsbA: a protein-folding catalyst contributing to bacterial virulence. *Microbes Infect.* **1**, 1221–1228 (1999).
45. Hiniker, A., Collet, J.F. & Bardwell, J.C. Copper stress causes an *in vivo* requirement for the *Escherichia coli* disulfide isomerase DsbC. *J. Biol. Chem.* **280**, 33785–33791 (2005).
46. Missiakas, D., Georgopoulos, C. & Raina, S. The *Escherichia coli dsbC* (*xprA*) gene encodes a periplasmic protein involved in disulfide bond formation. *EMBO J.* **13**, 2013–2020 (1994).
47. Thomas, W.E., Trintchina, E., Forero, M., Vogel, V. & Sokurenko, E.V. Bacterial adhesion to target cells enhanced by shear force. *Cell* **109**, 913–923 (2002).
48. Bann, J.G., Pinkner, J.S., Frieden, C. & Hultgren, S.J. Catalysis of protein folding by chaperones in pathogenic bacteria. *Proc. Natl. Acad. Sci. USA* **101**, 17389–17393 (2004).
49. Capitani, G., Eidam, O., Glockshuber, R. & Grütter, M.G. Structural and functional insights into the assembly of type 1 pili from. *Escherichia coli*. *Microbes Infect.* **8**, 2284–2290 (2006).
50. Collaborative Computational Project, Number 4. The CCP4 suite: programs for protein crystallography. *Acta Crystallogr. D Biol. Crystallogr.* **50**, 760–763 (1994).

Acknowledgments

This work was supported by the Swiss National Science Foundation (grants 310030B-138657 and 31003A-122095 to R.G.) and the Swiss Federal Institute of Technology Zürich within the framework of the Swiss National Center for Competence in Research Structural Biology Program. The PhD position of M.A.S. was supported by a grant from the Research Committee of the Paul Scherrer Institute (FK-05.08.1) to G.C.

Author contributions

The overall study was conceived and designed by M.D.C. and R.G. The biochemical experiments were performed by M.D.C. with contributions from C.P., M.A.S., O.E. and M.G.G., and G.C. contributed to the crystallographic structure determination, refinement and interpretation. M.D.C. and R.G. wrote the manuscript with the contribution of C.P., M.A.S. and G.C.

Competing financial interests

The authors declare no competing financial interests.

Additional information

Supplementary information is available in the online version of the paper. Reprints and permissions information is available online at http://www.nature.com/reprints/index.html. Correspondence and requests for materials should be addressed to R.G.